Estimation of coherence properties of an undulator-generated x-ray beam from near-field and far-field slit diffraction visibilities

V. L. R. Jacques,[1,2,3,*] D. Le Bolloc'h,[1] E. Pinsolle,[1,2] F.-E. Picca,[2] and S. Ravy[2]

[1]*Laboratoire de Physique des Solides (CNRS-UMR 8502), Bât. 510, Université Paris-sud, 91405 Orsay cedex, France*
[2]*Synchrotron SOLEIL, L'Orme des merisiers, Saint-Aubin BP 48, 91192 Gif-sur-Yvette cedex, France*
[3]*European Synchrotron Radiation Facility, 6 rue Jules Horowitz, BP220, 38043 Grenoble Cedex, France*

We report on the study of hard x-ray diffraction by slits from the Fresnel to the Fraunhofer regime. The dark spot, i.e., the position where a minimum of intensity is found in the center of the diffraction pattern, is clearly observed. By progressively tuning the degree of coherence of the incident beam, the effect of partial coherence on the diffraction patterns is studied. We show that the transverse coherence length can be deduced with a good accuracy from the visibility of fringes in the Fraunhofer regime. We also show that a good estimation of the transverse coherence length can be obtained from measurements in the Fresnel regime. The measurements are discussed in the framework of the Gaussian Schell-model. A high degree of coherence is reached at the sample position for a beam size of a few micrometers and allows high-quality coherence experiments.

I. DIFFRACTION FROM A PARTIALLY COHERENT BEAM: HOW TO MEASURE THE DEGREE OF COHERENCE FROM SLIT DIFFRACTION?

Coherent x-rays experiments are used in synchrotrons to address many scientific issues ranging from biology to hard and soft matter physics. This technique allows for instance one to perform imaging and strain mapping in materials using phase retrieval algorithms,[1–4] or to study slow dynamics in soft[5] and hard condensed matter.[6,7] This approach also allows to get unique information about the topology of isolated phase defects embedded in the probed volume as already shown in charge density wave systems,[8] in magnetic systems,[9] or in semiconductors.[10]

All such experiments require a good degree of coherence but synchrotron sources are hardly coherent themselves. However, micrometric transverse coherence lengths are obtained by letting the beam propagate over long distances and by using slits to collimate the beam far away from the sample position. As the partial coherence induces strong effects on the diffraction patterns, it is crucial to characterize it at the sample position.

One of the easiest experiments from which it is possible to estimate the transverse coherence length of the incident beam is Young's interference experiment using two holes. When the holes are infinitely small, the visibility of fringes is directly related to the degree of coherence of the incident beam. Several measurements and calculations[11] of spatial coherence properties have already been performed using dual apertures[12,13] or other interferometry methods.[14–17] However, Young's experiment is hard to perform in the x-ray regime. It requires a plate drilled with two very small and well defined holes ($\leqslant 1\,\mu$m) located less than $\approx 10\,\mu$m apart, i.e., the typical coherence length obtained in synchrotrons. By contrast, it is much easier to measure the single slit diffraction pattern in the Fraunhofer regime. We show here that it is possible to estimate the transverse coherence length from slit diffraction if few corrections are taken into account.

In the first part, we derive the formalism of partial coherence propagation to express the expected visibility as a function of coherence length in the far-field diffraction regime. Then we present measured diffraction patterns of hard x-rays by a slit, from the Fresnel to the Fraunhofer regime, and show that the evolution of the visibility is consistent with our calculations. The dark spot, i.e., the position where a minimum of intensity is measured at the center of the diffraction pattern, is clearly observed. By tuning the degree of coherence of the incident beam, the effect of partial coherence on the diffraction patterns is studied.

A. Propagation of a partially coherent beam

Getting a coherent beam at the sample position requires to fulfill a certain number of conditions. The volume of coherence is defined by three lengths: the temporal (or longitudinal) coherence length ξ_L, along the beam propagation vector $\mathbf{k}$, and two spatial (or transverse) coherence lengths ξ_T, in the two directions perpendicular to the direction of $\mathbf{k}$.[18,19] ξ_L is directly related to the monochromaticity of the beam and to the wavelength λ:

$$\xi_L = \frac{\lambda^2}{2\Delta\lambda}. \tag{1}$$

This parameter is difficult to adjust in a real experiment as it is fixed by the monochromator. It has to be compared to the maximum path length difference Δl between two beams. Interferences are possible if $\Delta l \leqslant \xi_L$. In a symmetric Bragg diffraction experiment, $\Delta l = 2\,\mu^{-1}\sin^2\theta$, where θ is the Bragg angle, and μ the linear absorption coefficient for a given material at a given energy. Working at small angles is then better to keep within the longitudinal coherence condition. The longitudinal coherence length can be measured by analyzing the contrast of fringes at several Bragg positions, as demonstrated recently.[20]

Contrary to ξ_L, the transverse coherence length ξ_T is an adjustable parameter. If one considers an incoherent source emitting homogeneously across a size S, ξ_T is inversely

proportional to the angular aperture of the source seen from a distance x:

$$\xi_T(x) = \frac{\lambda x}{S}. \tag{2}$$

In practice, it is more appropriate to take a gaussian distribution of intensity for the source, with a standard deviation σ:

$$\mathcal{G}(y_s) = \frac{1}{\sqrt{2\pi}\sigma} e^{-\frac{y_s^2}{2\sigma^2}}, \tag{3}$$

where y_s is the coordinate indexing the 1D source. In that case, the spatial coherence length at the distance x from the source reads

$$\xi_T(x) = \frac{\lambda x}{2\pi\sigma}. \tag{4}$$

The source is small enough at synchrotrons to get a reasonable coherence length at sample position. However, focusing optics such as mirrors are generally used in the optical setup. This introduces optical aberrations that affect the beam wavefront. To counterbalance this effect, secondary slits are used after the optical elements. If one considers these secondary slits as the new source, S is the secondary slits aperture in Eq. (2). As the two coherence lengths scale with λ, working at low energy increases the coherence volume.

Once a partially coherent beam is generated, either using the real or a secondary source, one has to select the coherent part of the beam with another set of slits just before the sample (the typical setup used for coherent x-rays experiments is displayed in Fig. 3). The important value to consider is the degree of coherence of the beam β, which represents the coherent part of the beam. It is defined at every distance x from the source as

$$\beta(x) = \frac{\xi_T(x)}{\phi(x)}, \tag{5}$$

where $\phi(x)$ is the beam size at position x. The degree of coherence of the x-ray beam can be tuned by changing the apertures of the two sets of slits.

More generally, the propagation of a beam from a partially coherent source can be described within the Gaussian Schell-model (GSM).[21] The mutual coherence function $\Gamma(y_{D_1}, y_{D_2})$ at two positions y_{D_1} and y_{D_2} on a plane perpendicular to the propagation direction and located at a distance D from the source is defined as

$$\Gamma(y_{D_1}, y_{D_2}) = \iint e^{-\frac{y_1^2 + y_2^2}{2\sigma^2}} e^{-\frac{(y_1 - y_2)^2}{2\xi_T^2}} e^{i(\varphi_1 - \varphi_2)} dy_1 dy_2, \tag{6}$$

where y_j denotes a position on the source plane and φ_j is the path length of the beam j ($j = 1,2$):

$$\varphi_j = \frac{2\pi}{\lambda} \left[(y_{D_j} - y_j)^2 + D^2 \right]^{1/2}. \tag{7}$$

In this paper, only the transverse coherence length is taken into account through the term $\exp[-(y_1 - y_2)^2/2\xi_T^2]$ in the integral of Eq. (6). The intensity calculated at a position y_D of the detector is then given by

$$I(y_D) = \Gamma(y_D, y_D). \tag{8}$$

It is interesting to note that in the GSM the degree of coherence β is constant for a free propagation: the beam size ϕ and ξ_T continuously increase with the same ratio.

B. Slit diffraction pattern from a partially coherent x-ray beam

From a theoretical point of view, Young's experiment is perfectly suited for the study of partial coherence. However, experimentally, in the x-ray regime, the diffraction by a rectangular aperture closed at a few micrometers and adjustable in size is much easier to perform. In the following, a detailed study of the slit diffraction phenomenon in condition of partial coherence is made.

The single slit diffraction is an atypical experiment. When slits are inserted in the path of a coherent beam, the phenomenon of diffraction is visible if the slit aperture a is of the same order of magnitude as ξ_T.[18,22] In that case, different diffraction regimes are observed depending on the wavelength, the slits aperture, and the distance D between the slits and the observation plane (see Fig. 1). The crossover distance between the Fresnel (near-field) and the Fraunhofer (far-field) regime is defined here as[23]

$$D_b \sim a^2/(2\pi\lambda). \tag{9}$$

The distance D_b corresponds to the distance where a minimum of intensity is observed at the center of the diffraction pattern [see Fig. 1(b)]. In the following, this position is called the *dark spot position* and it is equivalent to the Poisson bright spot observed for opaque objects.[24,25] In the near-field regime ($D \leqslant D_b$), the beam is quasiparallel, so that the distribution of
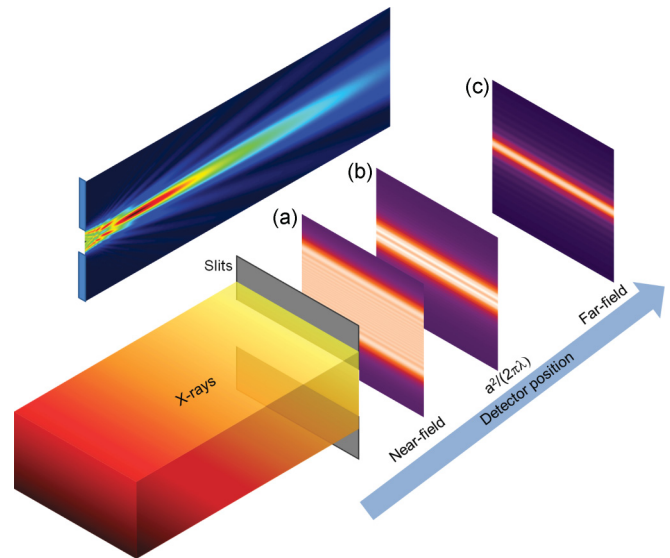

FIG. 1. (Color online) Distribution of intensity after diffracting slits. The image in the back illustrates this distribution along the beam propagation vector. The logarithmic color scale goes from dark blue for lowest intensities to dark red for highest intensities. (a)–(c) Measured distribution of intensity perpendicular to the beam propagation vector at different distances from the diffracting slits: (a) in the near-field regime, (b) at the dark spot position, and (c) in the far-field regime. The color scale for the maps goes from purple for lowest intensities to yellow for highest intensities. The distances as well as the sizes of the diffraction patterns are not to scale.

intensity is essentially limited by the slit aperture. In addition, some oscillations are visible on top of the slit profile, due to interferences between beams coming from each elemental surface of the diffracting slit. In the far-field regime ($D \gg D_b$), the beam diverges with an angle λ/a, and the intensity profile is given by the well-known cardinal sine squared function, i.e., the squared Fourier transform of a gate function: $I(x) \propto [\frac{\sin(\alpha x)}{\alpha x}]^2$, with $\alpha = \frac{\pi a}{\lambda D}$.

The fact that the beams effectively generated are not fully but only partially coherent affects the diffraction patterns. The degree of coherence of the x-ray beam can be tuned by changing the secondary slits aperture, for instance, and there are several ways to estimate the corresponding ξ_T. It can be estimated from the speckle pattern visibility in the small angle scattering obtained with disordered systems. In that case, β is related to the normalized variance of the speckle pattern intensity at a given wave vector.[26] ξ_T can also be measured from Young's experiment. The degree of coherence is related to the contrast of fringes V measured on the interference patterns and defined as[27]

$$V = \frac{I_{\max} - I_{\min}}{I_{\max} + I_{\min}}, \tag{10}$$

where $I_{\max}$ and $I_{\min}$ are adjacent local maxima and minima, respectively. As expressed by the Van Cittert-Zernike theorem, the visibility follows the Fourier transform of the Gaussian source distribution and is thus related to ξ_T and to the distance a between the holes as

$$V(\xi_T) = e^{-\frac{a^2}{2\xi_T^2}}. \tag{11}$$

In this case, the visibility is identical whatever the order of fringes from which it is measured. The situation is very different in the case of the diffraction by slits. In that case, the visibility cannot be defined the same way as in Young's experiment, because the contrast of fringes depends on where it is measured on the diffraction pattern, and is different in the near-field and the far-field diffraction regimes. Thus the effect of partial coherence on the diffraction patterns is not obvious. However, with some corrections performed on the measured diffraction patterns the coherence lengths can be estimated from the near-field and the far-field diffraction profiles.

Let us first consider the far-field diffraction regime. Calculations are performed using the GSM to estimate the evolution of the contrast of fringes in the case of a partially coherent beam. The diffraction patterns calculated from Eq. (6) for different ξ_T and keeping the same diffracting slit aperture are displayed in Fig. 2(a). The contrast of fringes decreases with decreasing coherence lengths, as expected. In all cases, the envelope is a squared hyperbola function [apart from the central maximum that display a gaussian profile (Guinier's law)[28]]: $(\alpha x)^{-2}$.

However, contrary to Young's experiment, the visibility of a sine cardinal squared function depends on the order of fringe from which it is measured. To obtain ξ_T from the diffraction patterns, independently on the location of the fringes, it is necessary to first normalize the diffraction profile by its squared hyperbola envelope [see inset of Fig. 2(b)]. The visibility obtained on the normalized curves as well as the visibility calculated from Eq. (11) are plotted with respect
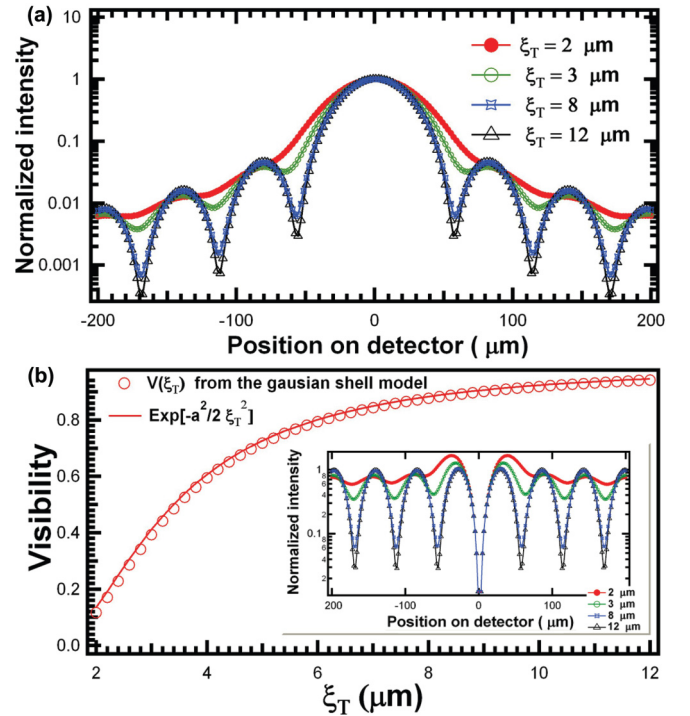

FIG. 2. (Color online) (a) Diffraction profile calculated from the GSM in the case of a rectangular slit, plotted for various ξ_T and for $a = 4$ μm, $\lambda = 1.5$ Å and a detector distance $D = 1.5$ m. $\alpha = \frac{\pi a}{\lambda D}$. The influence of the finite size of the source is neglected in Eq. (6). (b) Visibility vs ξ_T obtained from the normalized profiles (see text). (Inset) Normalized profiles displayed for different ξ_T. The central part has to be avoided to calculate the visibility.

to ξ_T in Fig. 2(b). The visibility of fringes is clearly related to ξ_T with the same law as in Young's experiment.

II. COHERENCE SETUP AT THE CRISTAL BEAMLINE OF THE SOLEIL SYNCHROTRON

The CRISTAL beamline is dedicated to diffraction. The source is an in-vaccum U20 undulator (20 mm magnetic period), standing in a short section of the storage ring. The vertical source size is 8.1 μm root mean square (rms) and the horizontal one 388 μm rms. The vertical divergence is 4.6 μrad rms and the horizontal one 14.5 μrad rms. A Si(111) double crystal monochromator is used as first optical element and can select beams with energies ranging from 4 to 30 keV. The second crystal of the monochromator is mounted on a bender for sagital focusing. The use of this monochromator fixes ξ_L for a given energy. At 8 keV, $\Delta\lambda/\lambda \approx 1.5 \times 10^{-4}$, leading to $\xi_L \sim 0.5$ μm. The monochromatic beam is then vertically focused by a first bendable mirror, coated with silicon, rhodium and platinum stripes in order to get a good harmonics rejection at any accessible energy with a constant deflection angle of 2.8 mrad. A second flat mirror with the same coatings deflects the beam back in the initial direction. Different sets of slits are then inserted in the beam path for collimation. We will concentrate in this paper on the slits located just after the mirrors, used as source slits and located at a distance $D_0 = 23$ m from the U20 undulator, and on another set located
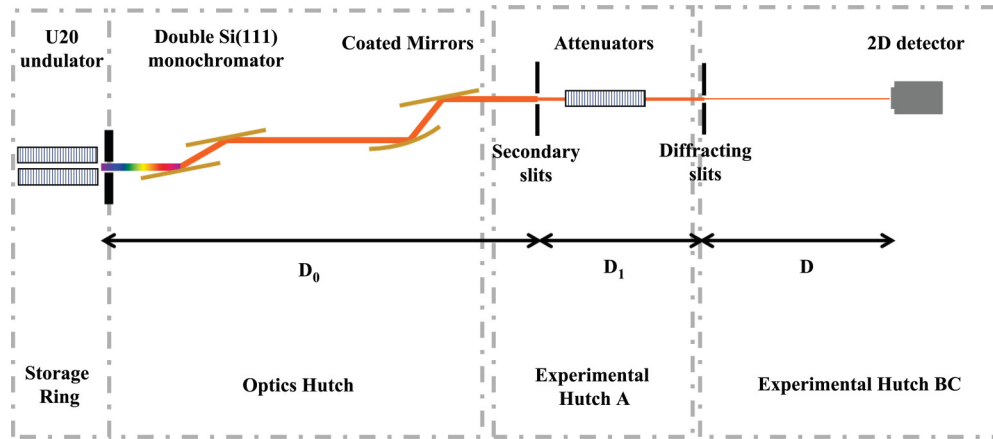
FIG. 3. (Color online) Scheme of the CRISTAL beamline layout used for the measurements reported here. Secondary slits and mirrors have been used for the experiment performed in the far-field only.

at a variable distance D_1 downstream of them, used to select the coherent part of the beam. Filters are inserted between the two sets of slits. Detection is performed at a distance D from the last slits using a 2D detector. This setup is illustrated in Fig. 3.

III. MEASUREMENT OF THE BEAM SPATIAL COHERENCE PROPERTIES

Two different measurements are presented in this section. The first one is performed in the far-field regime, where a cardinal sine squared function is observed. The second one is the measurement of the distribution of intensity from the near-field to the far-field regime. The link between measured visibilities and spatial coherence lengths is studied in the two regimes.

A. Linking visibility and coherence length in the far field

For this measurement, a 7.03 keV beam is selected ($\lambda = 1.763$ Å). The setup described in Fig. 3 is used with diffracting slits located at a distance $D_1 = 13$ m from the source slits. A deep depletion back-illuminated direct illumination Andor charge-coupled device (CCD) camera with 13 μm pixel size is installed at a distance $D = 1.5$ m from the diffracting slits for detection. The Droplet algorithm is used to treat the images.[29]

The real number of photons per pixel is thus retrieved. A diffraction pattern obtained with a diffracting slits aperture of 5×5 μm^2 is shown in Fig. 4 as well as a profile of the horizontal fringes.

Despite the fact that the synchrotron source emittance at Soleil is approximatively 100 times larger in the horizontal than in the vertical direction, the contrast of fringes is almost similar in the two directions. This is due to the fact that rectangular secondary slits are used.

The measurements have been performed with a diffracting slit aperture of 5 μm, i.e., twice less than the 10 μm slit size for which the limit of resolution is reached at this energy and this ratio between detector distance and pixel size. Several diffraction patterns have been recorded for different secondary slit sizes, and have been normalized by their squared hyperbola envelope, as explained before (see Fig. 5). The visibility is then calculated from the normalized diffraction patterns. The final visibility is obtained by averaging the local visibilities of these curves. The coherence length corresponding to each secondary slits aperture is calculated using Eq. (2). The measured normalized visibility as well as the expected law [see Eq. (11)] is plotted with respect to the obtained ξ_T in Fig. 5.

The overall evolution of the normalized visibility is in good agreement with the one expected from Eq. (11). For coherence
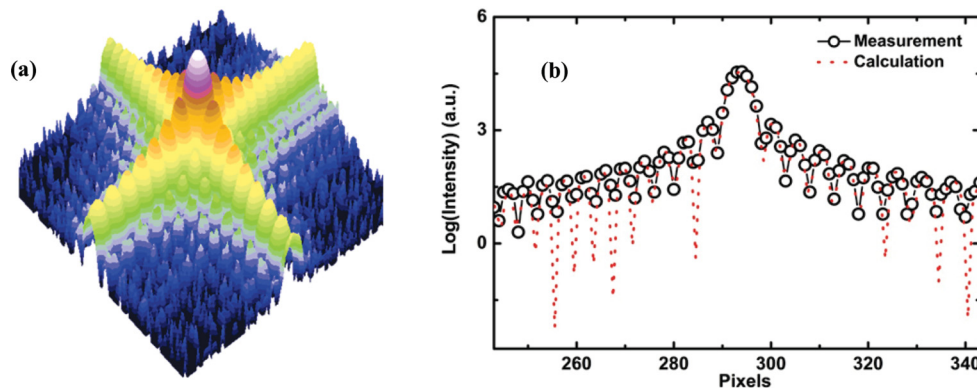

FIG. 4. (Color online) (a) Measured diffraction pattern obtained with a diffracting slits aperture of 5×5 μm^2, using the Andor CCD camera at a distance of 1.5 m from the slits (logarithmic scale). (b) Open circles: profile of the measured diffraction pattern shown in (a) along the horizontal direction (logarithmic scale). Red dotted line: calculation of the diffraction pattern using the real experimental conditions and considering a fully coherent beam.
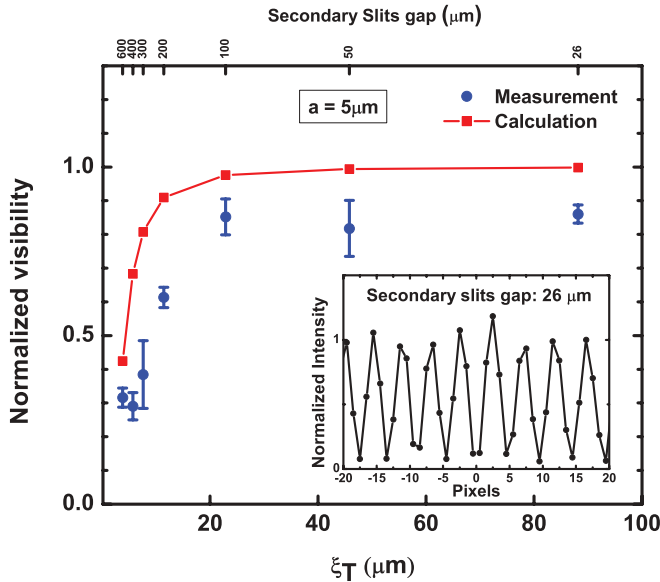
FIG. 5. (Color online) Evolution of the measured normalized visibility (blue dots) as well as the expected law given in Eq. (11) (red squares) with respect to the calculated coherence length. The corresponding secondary slits gap is indicated for each measured point on the upper x axis. (Inset) Measured diffraction profile obtained with a secondary slit aperture of 26 μm and normalized by the corresponding squared hyperbola envelope.

lengths smaller than ~ 7 μm, the visibility does not drop as much as expected. This is due to the fact that the beam is smaller than 400 μm at the secondary slits position, and thus, opening them further does not change the visibility on the recorded patterns.

On the other hand, the measured visibility is lower than the predicted one mainly because of the finite pixel size of the CCD detector. This is an important issue for x-ray diffraction experiments. Since the smallest pixel sizes available are around ten micrometers for direct-illumination x-ray CCD cameras, it is difficult to obtain more than five measured points per fringe with the experimental parameters used in Fig. 5. This low oversampling induces a lack of visibility

and thus an underestimation of the visibility. This effect can be estimated. Let us consider the initial periodic function $f(x) = 1 + \beta \cos(\frac{2\pi}{\eta} x)$ as the distribution of intensity, where η is the period of the oscillations. In principle, the calculation of the visibility V leads to $V = \beta$. When using a discrete camera, with pixel size b, the total intensity impinging the nth pixel results from an integration of the intensity over the pixel size:

$$I(n) = \int_{nb-\frac{b}{2}}^{nb+\frac{b}{2}} f(x)dx. \qquad (12)$$

The visibility is not equal to β anymore, but reads

$$V = \beta \frac{\sin\left(\frac{\pi b}{\eta}\right)}{\frac{\pi b}{\eta}}. \qquad (13)$$

In the measurements shown in Fig. 5, $\frac{b}{\eta} = \frac{1}{5}$ (five points per fringe). In that case, V is underestimated by $\sim 10\%$. Taking this correction into account, the measured visibilities are in good agreement with the expected ones.

In the far-field diffraction regime, the slit diffraction patterns can thus be used to estimate the coherence length during an experiment, provided a normalization by an envelope function is performed and the finite pixel size effect is taken into account. There are at least two advantages to favor the measurement with a slit than with a dual aperture. First, the flexibility of the slit gap allows one to adapt the aperture to the other parameters of the setup. Second, the same slit can be used for the estimation of the coherence properties of the beam and for the experiment itself to select the coherent part of the beam.

B. From the far field to the near field: estimation of the spatial coherence length

In this section, we show that it is possible to measure the distribution of intensity continuously from the far-field to the near-field regime. This continuous change is simply obtained by increasing the diffracting slit aperture and by using a high resolution detector. In addition, the measurement provides a good estimation of ξ_T.

Let us review the different ways of measuring the two regimes. The crossover distance between them is located at
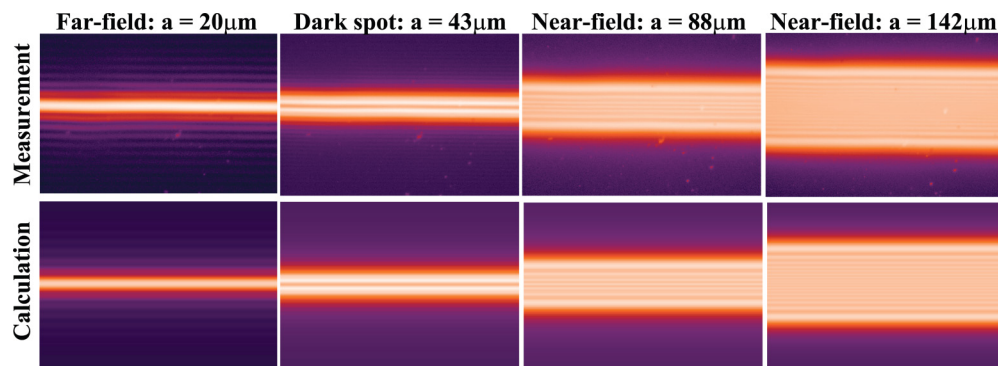

FIG. 6. (Color online) (Upper row) Measured diffraction patterns obtained for 4 different vertical slits gap, using a high resolution detector standing 3 m away from the slits (logarithmic scale). (Bottom row) Calculation of the profiles for the same apertures considering a fully coherent beam. The color scale goes from purple for lowest intensities to yellow for highest intensities. The dark spot is obtained for a diffracting slit aperture of $a_b = 43$ μm. The destructive interference in the middle is clearly visible. The near-field diffraction regime is obtained for slits apertures greater than a_b ($a = 142$ μm and $a = 88$ μm). The far-field regime is obtained for slits apertures lower than a_b ($a = 20$ μm).

a distance $D_b \sim a^2/(2\pi\lambda)$. One thus has three different ways to detect the two regimes. Either the slits-to-detector distance D is varied around D_b keeping a and λ fixed, or the detector is fixed at a certain distance from the slits and λ or a is varied.

Let us first consider the case where a and λ are fixed and the detector is moved through the boundary D_b. For $D \geqslant D_b$, the detector sits in the far-field regime. In our setup, the smallest available pixel size is around 1 micron, and the highest detector distance is 3 m. For D_b to be located at half the distance between slit and detector, one must have $a \sim \sqrt{2\pi\lambda D_b}$ i.e., $a \sim 30~\mu$m for $\lambda = 1$ Å. In these conditions, $\lambda(D - D_b)/a \sim 5~\mu$m, which is enough to resolve the fringes. However, if the detector is moved closer to the slits, the size of the beam is approximately the same as the slit itself, meaning that the distribution of intensity would spread over 30 pixels only. This would make difficult the observation of the fringes in the close vicinity of the slit.

The second possibility is to decrease the wavelength of the incoming beam to reach the Fresnel regime. Assuming a fixed detector at 3 m, and a slit aperture of 30 μm, having the detector in the near-field regime, e.g., $D_b = 2D$ implies using a 52 keV beam. Not only this energy is not accessible at the CRISTAL beamline but also the use of high energy is not favorable for

the transverse coherence length [ξ_T is proportional to λ, see Eq. (2)]. In addition, the transmitted beam at the edge of the blades of the slits could also reduce the visibility. One would in addition need a 2D detector able to cover a wide energy range to carry out the measurement.

The last possibility is to use a detector at a fixed position and a monochromatic beam, and change the aperture of the diffracting slit. This allows a fine tuning of the boundary distance between near-field and far-field regimes, and an easy observation of the interference fringes in both diffraction regimes.

However, this measurement requires a detector with a very good resolution. For this purpose, a $\lambda = 1$ Å monochromatic beam has been used, together with a 2D detector made of a YAG scintillator, lenses and a CCD camera. This detector provides an effective resolution of 1.3 μm and is located at a distance $D = 3$ m from the diffracting slits. The latter are used to cut the beam in the vertical direction only. The focusing mirrors are not inserted to avoid optical aberrations, meaning that only the monochromator and some filters are inserted in the beam, without focusing. The secondary slits are not used in this experiment. In these conditions, the source size to be considered is the real source one (the undulator), i.e., 8.1 μm rms. As the diffracting slits are located at 35 m from the source,
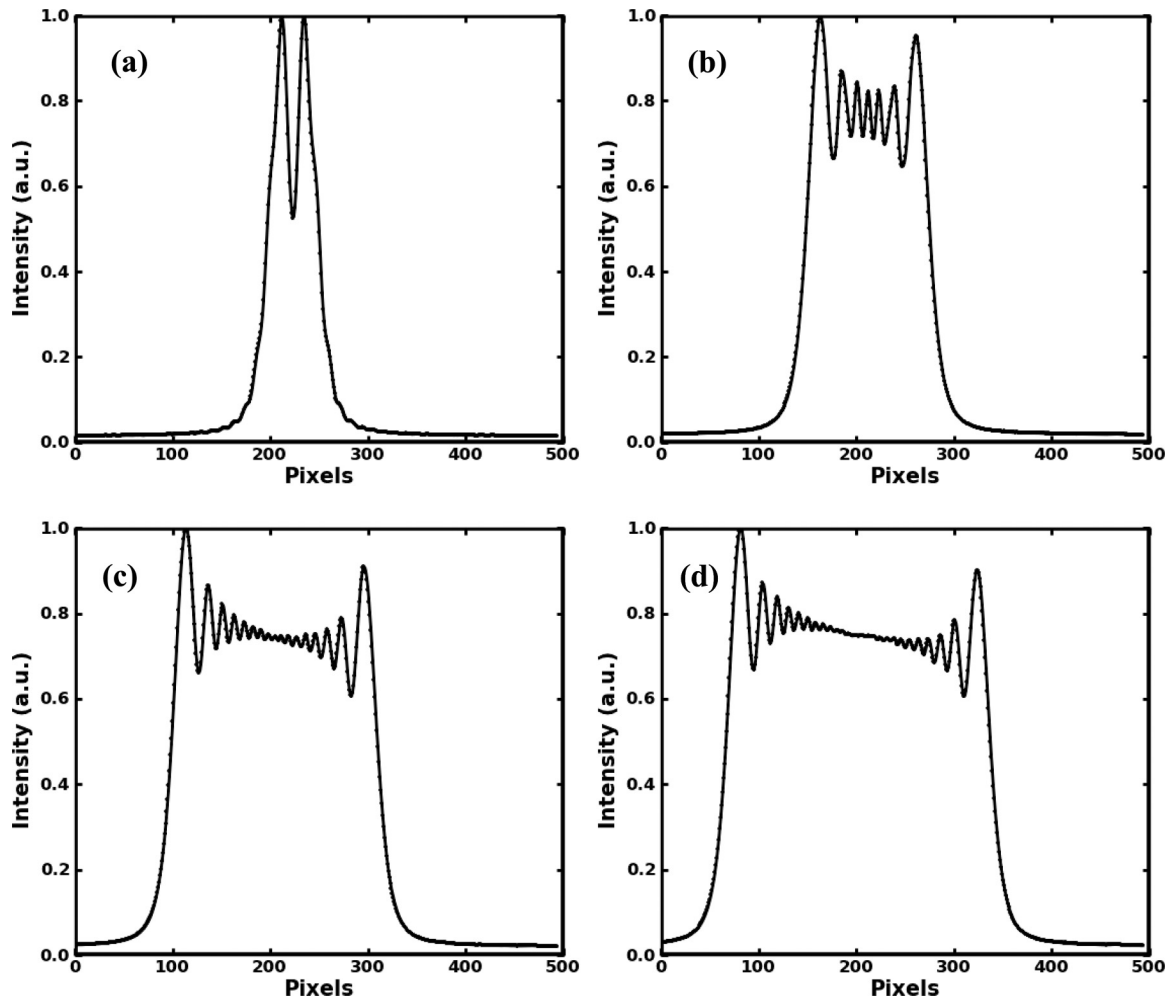

FIG. 7. Linear projection along the vertical direction of the distribution of intensity obtained in the near-field regime for different diffracting slits apertures: (a) $a = 43$, (b) 88, (c) 142, and (d) 182 μm. For large apertures, the asymmetry of the profile is probably due to a nonhomogeneous illumination of the slit.

the vertical coherence length at the slit position calculated from Eq. (4) is $\xi_T = 70\ \mu$m.

The diffracting slit aperture a has been varied from 1 μm to 300 μm by steps of 1 μm. The detector is exactly at the *dark spot* distance D_b when Eq. (9) is satisfied, i.e., for $a_b = 43\ \mu$m. The measurement thus contains both the near-field and the far-field diffraction regimes, as a has been varied below and above a_b. Some results are shown in Fig. 6 as well as calculations of the distribution of intensity after the slits for the same apertures in the case of a fully coherent beam. The complete measurement and calculation for each aperture are available as movies in Supplemental Material.[30]

In this measurement, the faint oscillations observed in the near-field regime are well reproduced by the simulation. The linear scale projection of the distribution of intensity along the horizontal direction of four maps taken in the near-field regime are displayed in Fig. 7. The oscillations appear clearly on these projections.

Defining the visibility in the near-field regime is not straightforward. It highly depends on the position where it is measured on the diffraction pattern. Here, the visibility of the oscillations V_e has been measured in the center of the distribution of intensity because this is where the oscillations are first blurred when opening the slits. V_e has been extracted for different slit gaps in the near-field regime ($a \geqslant a_b$) using Eq. (10). The visibility is plotted in the inset of Fig. 8 as a function of the diffracting slits gap for the points where a finite number of oscillations is recorded. The central fringes are not visible for gaps larger than 180 μm although the experimental resolution is good enough. This blurring effect is due to the finite value of the vertical transverse coherence length. The

study of the visibility should thus allow to get an estimation of ξ_T in the vertical direction. An analytical expression of the contrast in the center of the distribution can be derived from the asymptotic behavior of Fresnel integrals in the near-field diffraction regime (see Appendix). The exact central contrast can also be calculated numerically with Fresnel integrals. Here, a simulation of the expected distribution of intensity has been performed in the case of a partially coherent beam, using the GSM from Eq. (6). The detector point spread function is taken into account through a lorentzian convolution. The Lorentzian width has been evaluated by an adjustement at small apertures. In addition, the diffraction profile is asymmetric for large apertures (see Fig. 7). This effect is most probably due the nonhomogenous beam profile over such large apertures and is taken into account in the simulations. The measured contrast is well reproduced in the center of the distributions for a value $\xi_{T_G} = 50 \pm 5\ \mu$m. This value is less than the expected one ($\xi_T = 70\ \mu$m). Such mismatches have already been reported in previous works. In Ref. 17, this was attributed to a broadening of the effective source caused by the limited depth of focus of the electron beam in the storage ring at the undulator position. In our case, it is probably due to instabilities of the monochromator cooling system inducing vibrations, as also reported in Ref. 15.

It is interesting to note, however, that the evolution of the visibility with increasing apertures is well reproduced by a Gaussian function, like in the case of Young holes, if the measured visibility V_e is normalized by the calculated visibility V_t.[31] The latter is obtained considering a fully coherent beam and taking into account the detector point spread function and is in good agreement with the analytical expression of the central visibility V_a in the near-field regime limit (see calculations in Appendix). The evolution of V_e/V_t with increasing apertures then only depends on the finite value of ξ_T. V_e/V_t is plotted with respect to the diffracting slits aperture in Fig. 8. V_e and V_t are also shown on the inset of Fig. 8.

The normalized curve has the same Gaussian behavior like in the case of Young holes:

$$\frac{V_e}{V_t}(a) = e^{-\frac{a^2}{2\xi_{T_F}^2}},\qquad(14)$$

where ξ_{T_F} is the coherence length found with this model. The best fit yields $\xi_{T_F} = 58 \pm 2\ \mu$m (see Fig. 8). The value of ξ_{T_F} found with this methods is in good agreement with the value ξ_{T_G} obtained with the GSM.

IV. CONCLUSION

We have shown in this paper that the fine analysis of slit diffraction allows one to estimate the physical quantities characterizing the spatial coherence of the beam both in the near-field and far-field regime provided a few corrections are made to the measured recorded patterns. It is also noteworthy that the degree of coherence can reach very high values in some configurations of the optical setup, which allows getting a high visibility of the speckles during an experiment with a reasonable x-ray beam intensity. Within a double slits configuration, the use of focusing optics is crucial. It allows an increase of the flux density at the sample
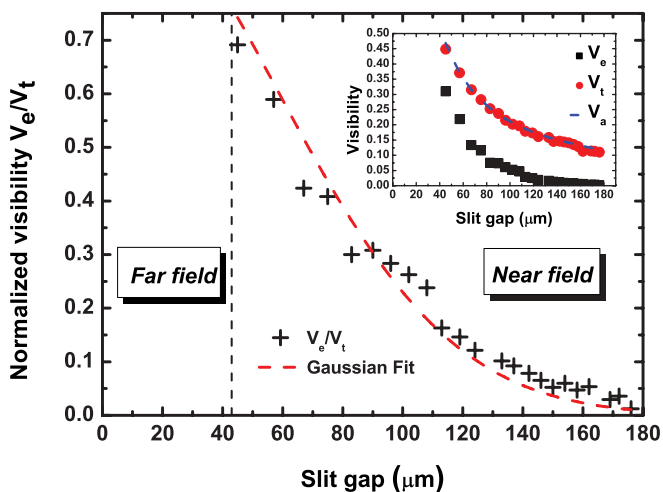
FIG. 8. (Color online) (Inset) Evolution of V_e (black squares), the visibility measured in the middle of the distribution of intensity and of V_t (red dots), the one calculated with the GSM, which takes into account the detector point spread function. Blue dashed line: envelope V_a of the calculated central visibility in the near-field regime limit (see Appendix). Normalized visibility V_e/V_t. The apertures were chosen so that an integer number of fringes appear in the distribution of intensity. The Gaussian fit was performed using Eq. (14) adding a constant background. The black dashed line shows the dark spot position, i.e., the crossover distance between near-field and far-field regimes.

position without decreasing much the transverse degree of coherence. The CRISTAL beamline is thus perfectly adapted to coherence studies, with adapted optical elements and detectors.

APPENDIX: ANALYTICAL CALCULATION OF THE CENTRAL VISIBILITY OF THE DIFFRACTION PATTERNS

In this Appendix, the analytical calculation of the visibility expected in the center of the slit diffraction pattern in the case of a point source is made. The exact expression in terms of Fresnel integrals as well as an estimation of the central visibility in the Fresnel regime are given. An expression similar to the one given in Ref. 30 is obtained, but for a factor of 2. Our result is consistent with the visibility calculated with the GSM (see text).

The coordinates along the diffracting slits are denoted y, and the ones on the detector plane x (see Fig. 9 for the notations).

The amplitude at the position x of the detector reads

$$A(x) = \int_{-a/2}^{a/2} e^{\frac{2i\pi}{\lambda}[\sqrt{r_s^2+y^2}+\sqrt{r_d^2+(x-y)^2}]} dy. \qquad (A1)$$

In our case, even in the near-field regime, we have $r_s \gg y$ and $r_d \gg x - y$. Thus the amplitude can be written as

$$A(x) \sim e^{\frac{2i\pi}{\lambda} r_t} \int_{-a/2}^{a/2} e^{\frac{i\pi}{\lambda r_s} y^2} e^{\frac{i\pi}{\lambda r_d}(x-y)^2} dy, \qquad (A2)$$

where $r_t = r_s + r_d$. Introducing the parameter a_0 defined as $a_0^2 = \frac{4\lambda r_d r_s}{r_t}$, one obtains

$$A(x) \sim \int_{-a/2}^{a/2} e^{\frac{i\pi}{2}(\frac{2\sqrt{2}}{a_0} y - \frac{a_0}{\sqrt{2}\lambda r_d} x)^2} dy \qquad (A3)$$
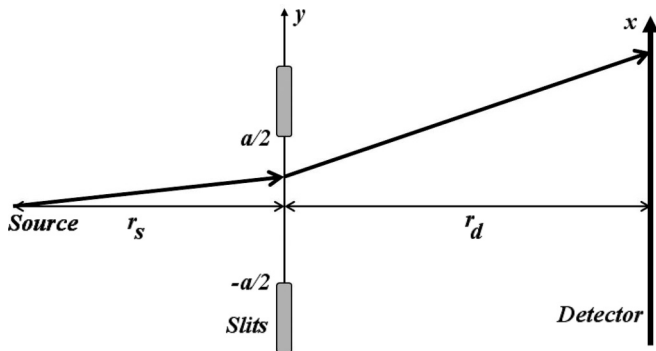

FIG. 9. Scheme of the layout and notations used for the calculation. The source is considered punctual, the slits are at a distance r_s from the source and the detector at a distance r_d from the slits.

in which phase prefactors have been omitted. After the change of variable $Y = \frac{2\sqrt{2}}{a_0} y - \frac{a_0}{\sqrt{2}\lambda r_d} x$, one obtains

$$A(x) \sim \frac{a_0}{2\sqrt{2}}[F(Y_0 - \delta x) + F(Y_0 + \delta x)], \qquad (A4)$$

where $Y_0 = \sqrt{2}\frac{a}{a_0}$, $\delta = \frac{a_0}{\sqrt{2}\lambda r_d}$, and $F(u) = \int_0^u e^{\frac{i\pi}{2} Y^2} dY$ are Fresnel integrals. The positions of the extrema, necessary for the calculation of the visibility, are the solutions of $\frac{\partial A(x)}{\partial x} = 0$, i.e., $x_n = \frac{n}{\delta Y_0}, n \in \mathbb{Z}$.

The central visibility is calculated using Eq. (10). A first extremum is found at $x_0 = 0$ ($n = 0$), where an amplitude $A_0(x_0) = \frac{a_0}{\sqrt{2}} F(Y_0)$ is found. The following extremum is found at $x_1 = \frac{1}{\delta Y_0}$ ($n = 1$), and an amplitude $A_1(x_1) = \frac{a_0}{2\sqrt{2}}[F(Y_0 - \frac{1}{Y_0}) + F(Y_0 + \frac{1}{Y_0})]$ is found at that position. The literal expression of the central visibility $V_l(a)$ can be numerically calculated using the Fresnel integrals and reads

$$V_l(a) = \left| \frac{|A_0(x_0)|^2 - |A_1(x_1)|^2}{|A_0(x_0)|^2 + |A_1(x_1)|^2} \right|. \qquad (A5)$$

The central visibility can be simplified in the near-field regime, in the limit $a \gg a_0$. In that case, the asymptotic behavior of the Fresnel integrals can be used: $F(u) = C(u) + iS(u)$ with $C(u) \approx \frac{1}{2} + \frac{1}{\pi u} \sin(\frac{\pi u^2}{2})$ and $S(u) \approx \frac{1}{2} - \frac{1}{\pi u} \cos(\frac{\pi u^2}{2})$ in the limit $u \gg 1$. In this limit, the intensities at the positions x_0 and x_1 read

$$I(x_0) = A(x_0)A^\star(x_0) \qquad (A6a)$$

$$\approx \frac{a_0^2}{2}\left[\frac{1}{2} + \frac{1}{\pi^2 Y_0^2} + \frac{\sqrt{2}}{\pi Y_0} \sin\left(\frac{\pi Y_0^2}{2} - \frac{\pi}{4}\right)\right] \qquad (A6b)$$

and

$$I(x_1) = A(x_1)A^\star(x_1) \qquad (A7a)$$

$$\approx \frac{a_0^2}{2}\left[\frac{1}{2} + \frac{1}{\pi^2 Y_0^2} - \frac{\sqrt{2}}{\pi Y_0} \sin\left(\frac{\pi Y_0^2}{2} - \frac{\pi}{4}\right)\right]. \qquad (A7b)$$
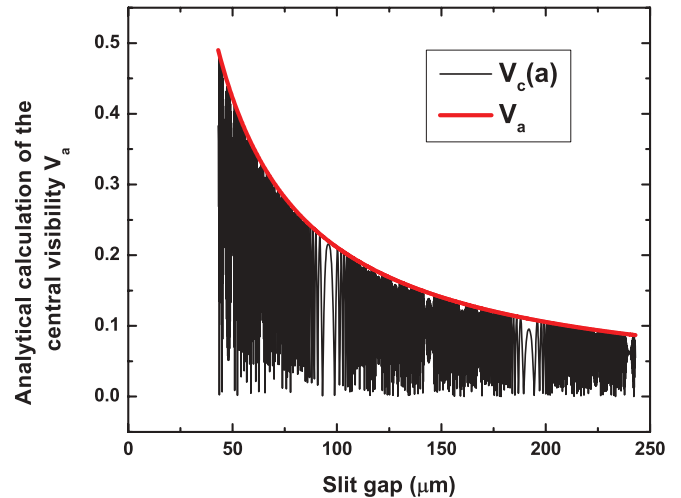

FIG. 10. (Color online) Black line: estimation of the central visibility $V_c(a)$ obtained analytically as a function of the slits gap in the near-field regime, in the approximation $a \gg a_0$. Red line: envelope V_a of the $V_c(a)$ function.

The central visibility $V_c(a)$ calculated within the approximation $Y_0 \gg 1$ thus reads

$$V_c(a) = \frac{2}{\pi} \frac{a_0}{a} \left| \cos\left[\pi\left(\frac{a^2}{a_0^2} - \frac{3}{4}\right)\right]\right|. \qquad (A8)$$

This function is rapidly oscillating with a, as shown in Fig. 10. The visibility obtained when a local maximum is found at $x = 0$ follows the envelope of $V_c(a)$: $V_a(a) = \frac{2}{\pi}\frac{a_0}{a}$, and is in good agreement with the visibilities obtained within the GSM (see Fig. 8), even in the regime $a \sim a_b$.

---

*vjacques@esrf.fr

[1] M. C. Newton, S. J. Leake, R. Harder, and I. K. Robinson, Nat. Mater. **9**, 120 (2010).

[2] M. Dierolf, A. Menzel, P. Thibault, P. Schneider, C. M. Kewish, R. Wepf, O. Bunk, and F. Pfeiffer, Nature (London) **467**, 436 (2010).

[3] P. Godard, G. Carbone, M. Allain, F. Mastropietro, G. Chen, L. Capello, A. Diaz, T. Metzger, J. Stangl, and V. Chamard, Nat. Commun. **2**, 568 (2011).

[4] J. Miao, R. Sandberg, and C. Song, IEEE J. Sel. Top. Quantum Electron. **18**, 399 (2012).

[5] A. Duri, T. Autenrieth, L.-M. Stadler, O. Leupold, Y. Chushkin, G. Grübel, and C. Gutt, Phys. Rev. Lett. **102**, 145701 (2009).

[6] S. Streit, C. Gutt, V. Chamard, A. Robert, M. Sprung, H. Sternemann, and M. Tolan, Phys. Rev. Lett. **98**, 047801 (2007).

[7] K. Ludwig, F. Livet, F. Bley, J.-P. Simon, R. Caudron, D. Le Bolloc'h, and A. Moussaid, Phys. Rev. B **72**, 144201 (2005).

[8] D. Le Bolloc'h, S. Ravy, J. Dumas, J. Marcus, F. Livet, C. Detlefs, F. Yakhou, and L. Paolasini, Phys. Rev. Lett. **95**, 116401 (2005).

[9] V. L. Jacques, D. Le Bolloc'h, S. Ravy, C. Giles, F. Livet, and S. B. Wilkins, Eur. Phys. J. B **70**, 317 (2009).

[10] V. L. R. Jacques, S. Ravy, D. Le Bolloc'h, E. Pinsolle, M. Sauvage-Simkin, and F. Livet, Phys. Rev. Lett. **106**, 065502 (2011).

[11] I. A. Vartanyants and A. Singer, New J. Phys. **12**, 035004 (2010).

[12] F. T. S. Yu and Y. W. Zhang, Appl. Opt. **25**, 3191 (1986).

[13] D. Ambrosiniy, G. Schirripa Spagnoloy, D. Paolettiy, and S. Vicalviz, Pure Appl. Opt. **7**, 933 (1998).

[14] J. J. A. Lin, D. Paterson, A. G. Peele, P. J. McMahon, C. T. Chantler, K. A. Nugent, B. Lai, N. Moldovan, Z. Cai, D. C. Mancini *et al.*, Phys. Rev. Lett. **90**, 074801 (2003).

[15] P. Cloetens, J. P. Guigay, C. De Martino, J. Baruchel, and M. Schlenker, Opt. Lett. **22**, 1059 (1997).

[16] K. Tamasaku and T. Ishikawa, Acta Crystallogr. Sect. A **57**, 197 (2001).

[17] M. Pfeifer, G. Williams, I. Vartanyants, R. Harder, and I. Robinson, Nature (London) **442**, 63 (2006).

[18] M. Born and E. Wolf, *Principles of Optics* (Pergamon Press, 1975).

[19] S. K. Sinha, M. Tolan, and A. Gibaud, Phys. Rev. B **57**, 2740 (1998).

[20] S. Leake, M. Newton, R. Harder, and I. Robinson, Opt. Express **17**, 15853 (2009).

[21] L. Mandel and E. Wolf, *Optical Coherence and Quantum Optics* (Cambridge University Press, 1995).

[22] D. Le Bolloc'h, F. Livet, F. Bley, T. Schulli, M. Veron, and T. H. Metzger, J. Synchrotron Radiat. **9**, 258 (2002).

[23] This expression differs slightly from the usual expression $D_b \sim a^2/(4\lambda)$. We choose here to define the crossover distance where the clearly visible dark spot appears.

[24] A. Fresnel, *Oeuvres complètes 1* (Imprimerie impériale, Paris, 1868).

[25] D. Le Bolloc'h and J. Sadoc, Eur. Phys. J. B: Complex Syst. **81**, 481 (2011).

[26] F. Livet, Acta Crystallogr. Sect. A **63**, 87 (2007).

[27] M. Born and E. Wolf, *Principles of Optics Electromagnetic Theory of Propagation, Interference and Diffraction of Light* (Pergamon Press, New York, NY, 1964).

[28] A. Guinier, *X-ray Diffraction in Crystals, Imperfect Crystals and Amorphous Bodies* (General Publishing Company, Toronto, 1994).

[29] F. Livet, F. Bley, M. Sutton, J. Mainville, E. Geissler, G. Dolino, and R. Caudron, Nucl. Instrum. Meth. A **451**, 596 (2000).

[30] See Supplemental Material at http://link.aps.org/supplemental/10.1103/PhysRevB.86.144117 for the continuous change of the pattern from the far-field to the near-field regime. On the measured patterns, the central fringes get blurred for big enough apertures.

[31] V. Kohn, I. Snigireva, and A. Snigirev, Phys. Rev. Lett. **85**, 2745 (2000).